Optics and Spectroscopy, 2025, Vol. 133, No. 11

10

Pulse characteristics of single-junction and triple-junction laser photoconverters

© V.S. Kalinovskii, I.A. Tolkachev, E.V. Kontrosh, K.K. Prudchenko, V.S. Yuferev, S.V. Ivanov

Ioffe Institute,
St. Petersburg, Russia

e-mail: vitak.sopt@mail.ioffe.ru

Received May 07, 2025
Revised August 31, 2025
Accepted October 24, 2025

The pulsed photoresponse characteristics of a single-junction (SJ) and a triple-junction (TJ) monolithic GaAs/AlGaAs $p-i-n$ photoconverters (Ø250 μm) (PCs) in the photovoltaic mode under excitation by pulsed laser irradiation with $\lambda = 850$ nm were investigated. The peak radiation power density (P_{p}) was varied up to 9.6 kW/cm^2 at a pulse duration of 140 ps. It is shown that the photoresponse pulse broadening for a SJ PCs is due to the influence of the electric field collapse of the $p-i-n$ junction at $P_{\text{p}} \geq 1.1$ kW/cm^2. In the photovoltaic mode, the possibility of increasing the fast performance at P_{p} up to 9.6 kW/cm^2 by using the TJ PCs mounted by vacuum soldering on a ceramic microstrip heat sink base has been demonstrated.

Keywords: pulse characteristics, single-junction and triple-junction monolithic $p-i-n$ photoconverters, collapse of the electric field, vacuum soldering.

DOI: 10.61011/EOS.2025.11.62913.8140-25

Currently, radiophotonics is actively developing as a scientific and technical field. One of its key elements is the powerful pulsed photoconverter (PC), used, for example, in radiophotonic phased antenna arrays [1–4]. The efficiency of radiophotonic phased antenna arrays is determined by a combination of parameters: the electrical power of the PC, its speed, matching with the parameters of the external load (e.g., an antenna), and the autonomy of the power system, which provides complete galvanic isolation between the radiator — antenna array and the main generating equipment. In this case, the PC must efficiently convert subnanosecond optical pulses with minimal delay in the photovoltaic mode (without reverse bias voltage). Various sources describe PC designs operating in diode mode with applied reverse bias. These include $p-i-n$-PCs [5,6], unipolar PCs [7–9], and modified unipolar PCs [10], in which the key feature is the presence of an undoped (unipolar PCs) $p-i-n$ or lightly doped (modified unipolar PCs) micron- or submicron-thick i-layer.

A promising and more efficient method for converting pulsed laser radiation into microwave signals is the use of monolithic multi-junction $p-i-n$ PCs (MJ PCs) MJ PCs consist of photoactive $p-i-n$-sub-elements with the same bandgap width but different thicknesses of the photoactive layers, connected in series via tunnel diodes [11]. The monolithic connection of sub-elements in MJ PCs allows for increased optical excitation levels, reduced electrical and optical losses, higher amplitude of the electrical signal, and better matching with the load.

The aim of this work is to investigate the pulse characteristics of single-junction $p-i-n$ AlGaAs/GaAs PCs (SJ PCs) and compare the results with the pulse characteristics of triple-junction AlGaAs/GaAs PCs (TJ PCs) operating in the photovoltaic mode under excitation from a multimode optical fiber with a diameter of 50 μm by 140 ps laser pulses at a wavelength of 850 nm and varying power densities.

The technological schemes of the SJ and TJ PC structures are described below, i.e., the sequence of epitaxial layers with their initial thicknesses, compositions, and doping levels specified by technologists during the epitaxial growth process. It is important to note that during growth, the PC structure is subjected to thermal exposure, which leads to thermal diffusion of impurity atoms, resulting in changes to the parameters specified in the technological scheme relative to their initial values. Therefore, the modeling accounted for both the initial technological growth scheme of the PC structure and parameters obtained directly from the epitaxial structure using secondary ion mass spectrometry (SIMS). The technological scheme of the SJ PC structure included a contact layer of p^+-GaAs, doped at $N_A \sim 7 \cdot 10^{19}$ cm^{-3}, with a thickness of 0.4 μm, a wide-bandgap window consisting of p-Al$_{0.6}$Ga$_{0.4}$As ($N_A \sim 1 \cdot 10^{19}$ cm^{-3}) and p-Al$_{0.12}$Ga$_{0.8}$As ($N_A \sim 5 \cdot 10^{19}$ cm^{-3}) with thicknesses of 0.04 and 2 μm respectively, an emitter p-GaAs-layer ($N_A > 1 \cdot 10^{18}$ cm^{-3}) with a thickness of 0.7 μm, i-GaAs-layer ($N_D \sim 1 \cdot 10^{15}$ cm^{-3}) with a thickness of 1 μm, and a base n-GaAs-layer ($N_D \leq 1 \cdot 10^{18}$ cm^{-3}) with a thickness of 0.5 μm, followed by a Bragg reflector and a buffer n^+-AlAs/GaAs-layer ($N_D \sim 2 \cdot 10^{18}$ cm^{-3}) on an n^+-GaAs-substrate ($N_D \sim 2 \cdot 10^{18}$ cm^{-3}).

The technological scheme of the monolithic TJ PC structure had an identical contact layer to the SJ PC, a single-layer wide-bandgap p-Al$_{0.3}$Ga$_{0.7}$As-window ($N_A \sim 5 \cdot 10^{19}$ cm^{-3}) with a thickness of 0.3 μm and three

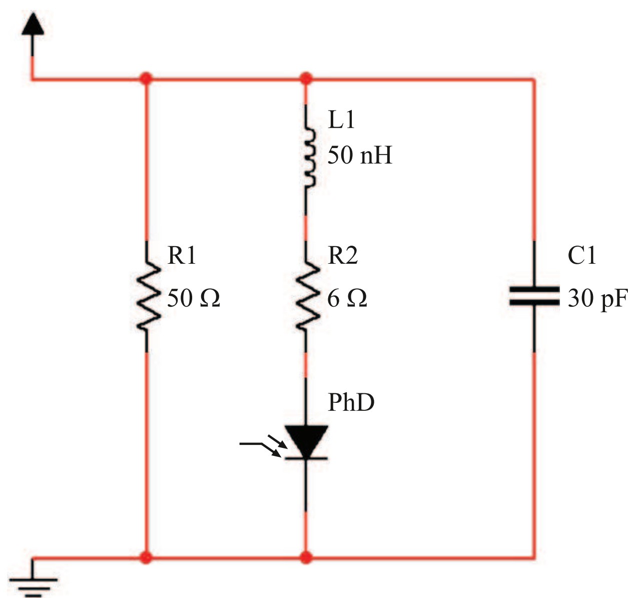

Figure 1. Electrical circuit of a single-junction $p-i-n$ AlGaAs/GaAs-PC, where R_1 is the load resistance, and R_2, L_1 and C_1 are the parasitic resistance, inductance, and capacitance, respectively, due to the mounting of the SJ PC on a microstrip line.

$p-i-n$-sub-elements with the same doping levels as the SJ PC. The thicknesses of the top, middle, and bottom photoactive junctions were 0.38, 0.62, and 2.02 μm respectively, and were determined based on the condition of equal photocurrents [12] generated in the sub-elements at the laser wavelength. The structure also included a back-surface field barrier of n-$Al_{0.3}Ga_{0.7}As$ and was grown on an n^+-GaAs-substrate ($N_D \sim 2 \cdot 10^{18}$ cm^{-3}). Back-to-back tunnel GaAs $p^{++}-n^{++}$ diodes with thicknesses of ≤ 30 nm were used as interconnects between the photoactive $p-i-n$-junctions. The diameter of the photoactive mesa surface of the investigated samples was 250 μm. In [12] it was shown that TJ PCs in the power density range of ≤ 2 mW/cm^2 for continuous-wave laser radiation at $\lambda = 850$ nm had open-circuit voltages of 1.82 V and electrical power of 0.34 mW/cm^2 at an efficiency of 18.3%, surpassing the characteristics of SJ PCs (efficiency 17%) grown by MBE and fabricated using identical technological processes with the same chip geometry at the same optical power.

The reliability and performance characteristics of modern high-power semiconductor devices with significant heat generation are largely determined by the efficiency of heat dissipation [13]. To ensure efficient heat dissipation and matching with the 50 Ω load, the PCs were mounted by vacuum soldering onto a symmetric microstrip line formed on a ceramic heat-sinking AlN substrate under conditions that do not degrade the PC structure characteristics. Soldering of the PCs was performed onto identical heat-sinking substrates with pre-deposited metal contacts. Multilayer Ti/Cu/Ni/Au contacts with a total thickness of ~ 5 μm were formed on the ceramic, and the back contact to the PC (Au(Ge)/Ni/Au) had a final gold layer of ~ 0.2 μm. Soldering was carried out in vacuum using Sn42%Bi58% paste (KOKI TB48-M742) in accordance with the manufacturer's recommendations [14] and a technology developed based on prior studies using laser scanning photodeflection microscopy with optimization of the thermal conductivity coefficient of the soldered layer [15,16]. The studies showed that for optimal heat dissipation when selecting solder paste and soldering conditions, the actual thermal characteristics of the solder layers must be considered, as they can differ significantly from those of the base multicomponent alloys.

Front contact leads for the PCs were made by ultrasonic welding of 50 μm gold wire to minimize parasitic inductances.

In calculating the pulse characteristics, the electrical circuit shown in Fig. 1 was taken into account, including both the 50 Ohm load resistance and the parasitic resistance, inductance, and capacitance due to mounting the SJ PC on the microstrip line. The circuit parameters were obtained according to the method described in [17].

During the work, photoresponse pulses of the SJ PC (Fig. 2, curves *1, 2*) for the structure under consideration (table) were measured, which retain the photoresponse shape and speed up to a certain optical power density level, after which saturation occurs. To understand the cause of saturation, numerical modeling of photoresponse pulses for a similar SJ PC structure under subnanosecond pulses of constant duration at the same laser power density levels as in the experiment was performed (Fig. 2, curves *1', 2'*).

In the mathematical modeling of SJ and TJ PC photoresponse pulses in the photovoltaic mode, structure parameters were used from the epitaxial growth technological scheme excluding the top contact layers, as they do not

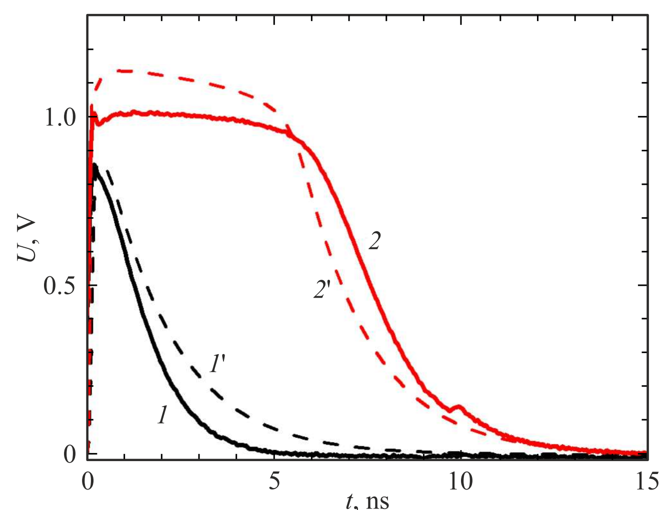

Figure 2. Comparison of experimental (curves *1, 2*) and simulated ($1'$, $2'$) photoresponse pulses of a single-junction $p-i-n$ AlGaAs/GaAs-PC under laser excitation ($\lambda = 850$ nm, $\tau_{0.5} = 140$ ps): curves *1, 1'*-1.14 kW/cm^2, curves *2, 2'* — 5.3 kW/cm^2.

Parameters of photoresponse pulses for experimental and simulated structures based on data from the epitaxial growth technological scheme and SIMS for single-junction and triple-junction monolithic $p-i-n$ AlGaAs/GaAs-PC

№	Structure	P_{peak}, kW/cm^2	U_{max}, V	$\tau_{0.5}$, ns	Note
1	SJ $p-i-n$-PC, experiment	1.14	0.857	1.46	
		5.3	1.015	7.54	
2	SJ $p-i-n$-PC, calculation	1.14	0.865	1.73	Technological scheme
		5.3	1.139	6.48	
3	TJ $p-i-n$-PC experiment	9.6	2.7	0.74	
4	TJ $p-i-n$-PC, calculation	5.3	3.2	0.99	Process flow diagram
		5.3	3.1	0.91	SIMS
		9.6	3.3	1.5	Process flow diagram
		9.6	3.4	1.38	SIMS

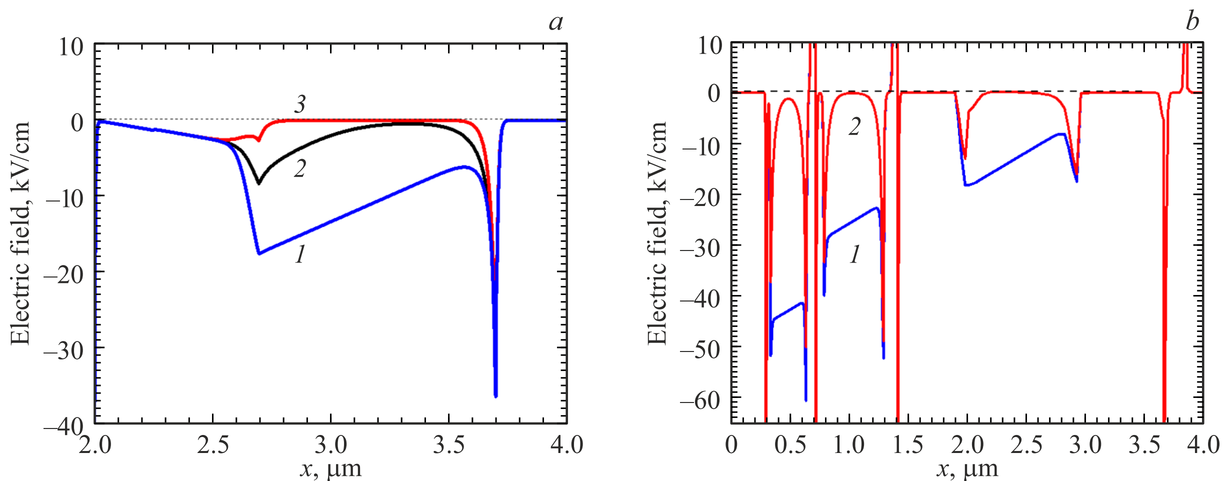

Figure 3. Electric field strength distribution across the space-charge region (SCR): (*a*) SJ $p-i-n$ AlGaAs/GaAs-PC: *1*—moment of optical excitation onset, (*2, 3*) — at the peak of the photoresponse pulse amplitude at laser power densities of 1.14 kW/cm^2 (*2*) and 5.3 kW/cm^2 (*3*), (*b*) TJ $p-i-n$ AlGaAs/GaAs-PC based on technological parameters: *1*—moment of optical excitation onset, *2*—at the peak of the photoresponse pulse amplitude under 5.3 kW/cm^2 excitation.

directly participate in charge carrier generation [18]. It was shown that in the simulated SJ PC at a laser power density of 5.3 kW/cm^2 saturation of the pulse amplitude occurs with strong broadening of the photoresponse duration at half-maximum to 7.54 ns (table, Fig. 2, curve *2'*). Comparing the obtained photoresponse pulses with theoretical calculations reveals qualitative agreement, though the simulated pulses have slightly higher amplitudes than the experimental ones. This can be explained by several factors: first, differences between technological parameters and those of the actual experimental structure; second, neglect of PC thermal heating in the calculations; third, neglect of the laser intensity density distribution across the PC photoactive surface. The observed saturation of amplitude and increase in photoresponse pulse duration are explained by the electric field collapse in the SJ PC [19]. Fig. 3, *a* shows the electric field strength distributions in the space-charge region (SCR) of the SJ PC calculated at different times and laser power density levels. It is evident that at 1.14 kW/cm^2 the electric field decreases but remains sufficient for charge separation, so current saturation does not occur. However, at 5.3 kW/cm^2 the electric field strength in the SCR becomes nearly zero, resulting in the collapse of the built-in electric field's ability to separate charges in the $p-i-n$ junction. This leads to saturation regime, limiting the photoresponse pulse

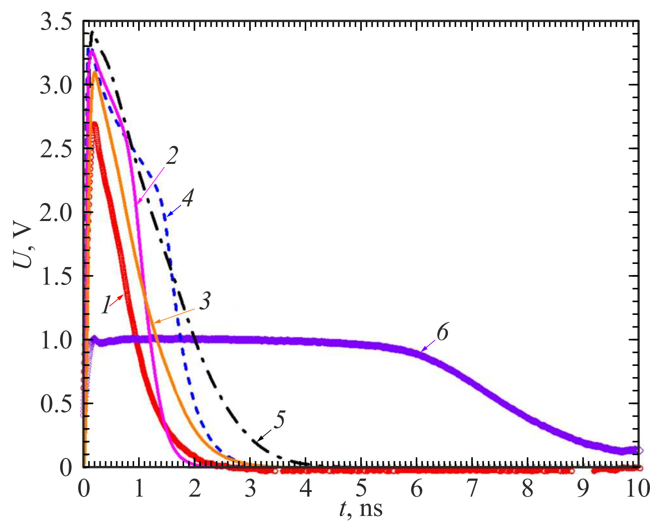

Figure 4. Experimental (curves *1, 6*) and calculated (*2–5*) photoresponse pulse characteristics of TJ PC (*1–5*) and SJ PC (*6*) at optical power densities of 5.3 kW/cm^2 (*2, 3, 6*) and 9.6 kW/cm^2 (*1, 4, 5*), where curves *2, 4* are calculated using technological scheme parameters, and *3, 5* using SIMS measurements.

amplitude growth to ~ 1 V with a substantial increase in the output electrical pulse duration of the SJ PC to $\tau_{0.5} \sim 7.54$ ns due to the dominance of diffusion and reduction of drift transport mechanisms through the SCR. The situation changes when the same power is applied to the TJ PC. Fig. 3, *b* presents the electric field strength distributions in the SCR at a laser power density of 5.3 kW/cm^2.

The field collapse observed in the SJ PC at a laser power density of 5.3 kW/cm^2 leads to a strong increase in $\tau_{0.5}$ — the pulse duration (Fig. 2, curve *2*), whereas in the triple-junction $p-i-n$-AlGaAs/GaAs-PC, this is not explicitly observed at power densities up to ~ 9.6 kW/cm^2. From Fig. 3, *b*, it is seen that at 5.3 kW/cm^2 the electric field strength does not drop to zero, remaining at 1.2 kV/cm in the front $p-i-n$ junction. The photoresponse pulse shapes for the investigated PCs and their parameters are shown in Fig. 4 (curves *1, 4*) and given in the table. Field collapse in the TJ PC at a laser power density of ~ 9.6 kW/cm^2 is explicitly absent; the photoresponse pulse amplitude is 2.7 V with a half-maximum duration of $\tau_{0.5} \sim 740$ ps (Fig. 4, table).

The TJ PC photoresponse pulse shapes obtained from calculations at a laser power density of 9.6 kW/cm^2 are shown in Fig. 4, where curve *4* uses parameters from the technological scheme and curve *5* uses SIMS measurements. The pulse parameters are summarized in the table. Differences in the amplitudes of simulated photoresponse pulses from the experiment for the TJ PC can be explained by the same factors noted earlier for the SJ PC.

Thus, the pulse photoresponse characteristics of SJ and TJ PCs in the photovoltaic mode under 850 nm laser excitation with $\tau_{0.5} = 140$ ps pulses and power densities up to 9.6 kW/cm^2 were investigated. Calculations in modeling the SJ PC structure showed that photoresponse pulse broadening at a laser power density of ≤ 5.3 kW/cm^2 is associated with electric field collapse in the space-charge region of the $p-i-n$-AlGaAs/GaAs-PC.

In the monolithic TJ $p-i-n$-AlGaAs/GaAs-PC converting pulsed laser radiation in the photovoltaic mode at 850 nm with power densities up to 9.6 kW/cm^2 explicit electric field collapse is absent, and the amplitude of the generated subnanosecond-range electrical pulse increases proportionally to the number of photoactive $p-i-n$-AlGaAs/GaAs-junctions.

Funding

The work was supported by a grant from the Russian Science Foundation No. 24-19-00716 (https://rscf.ru/project/24-19-00716).

Conflict of interest

The authors declare that they have no conflict of interest.

References

[1] D.F. Zaitsev, V.M. Andreev, I.A. Bilenko, A.A. Berezovskii, P.Yu. Vladislavskii, Yu.B. Gurfinkel', L.I. Tsvetkova, V.S. Kalinovskii, N.M. Kondrat'ev, V.N. Kosolobov, V.F. Kurochkin, S.O. Slipchenko, N.V. Smirnov, B.V. Yakovlev. Radiotekhnika, **85** (4), 153 (2021). (in Russian). DOI: 10.18127/j00338486-202104-17

[2] L.D. Bakhrakh, D.F. Zaitsev. DAN, **394** (4), 465?468 (in Russian).

[3] D.F. Zaitsev, Patent RU2298810, (2005). (in Russian)

[4] D.F. Zaitsev. Nanofotonika i ee primenenie (Akteon, M., 2014) p.445. (in Russian).

[5] T. Nagatsuma, H. Ito, T. Ishibashi. Laser & Photon, **3** (1–2), 123?137 (2009). DOI: 10.1002/lpor.200810024/

[6] A. Rawat, M. Saif Islam. Proc. SPIE, 12880, 128800Q (2024). DOI: 10.1117/12.3003413

[7] H. Ito, T. Furata, S. Kodama, T. Ishibashi. Electron. Lett., **36**, 1809–1810 (2000). https://doi.org/10.1049/el:20001274

[8] I.B. Chistokhin, K.S. Zhuravlev. **3** (1), p. 85–94 (2015). (in Russian)

[9] D. Maes, S. Lemey, G. Roelkens, M. Zaknoune, V. Avramovic, E. Okada, P. Szriftgiser, E. Peytavit, G. Ducournau, B. Kuyken. APL Photonics **8**, 016104, (2023). DOI: 10.1063/5.0119244

[10] Y. Peng, K. Sun, Y. Shen, A. Beling, J. C. Campbell. Optics express. **28** (19), 28563–28572 (2020). DOI: 10.1364/OE.399102

[11] V.S. Kalinovskiy, E.V. Kontrosh, G.A. Gusev, A.N. Sumarokov, G.V. Klimko, S.V. Ivanov, V.S. Yuferev, T.S. Tabarov, V. M. Andreev. Journal of Physics: Conf. Series, **993** 012029, (2018). DOI: 10.1088/1742-6596/993/1/01202

[12] V.S. Kalinovskii, E.V. Kontrosh, I.A. Tolkachev, K.K. Prudchenko, S.V. Ivanov. Pisma v ZhTF **50** (22), 35–38 (2024). (in Russian)

[13] J. Mathew, S. Krishnan. J. of Electronic Packaging, **144**, 010801 (2022). DOI: 10.1115/1.4050002

[14] Koki Company Limited [Electronic resource], http://www.koki.org/pdf/B1-07_TB48-M742_E.pdf
[15] A.L. Glazov, V.S. Kalinovskii, E.V. Kontrosh, K.L. Muravikov. Pisma v ZhTF, **48** (22), 39–42 (2022). (in Russian) DOI: 10.21883/PJTF.2022.22.53806.19338
[16] A.L. Glazov, V.S. Kalinovskii, A.A. Kapralov, E.V. Kontrosh, K.L. Muravikov, K.K. Prudchenko. Pisma v ZhTF, **51** (4), 31–34 (2025). DOI: 10.61011/PJTF.2025.04.59840.20123
[17] E.V. Kontrosh, V.V. Lebedev, G.V. Klimko, V.S. Kalinovskii, V.M. Andreev. J. Phys.: Conf. Ser., **697** 012185, (2020). DOI: 10.1088/1742-6596/1697/1/012185
[18] V.S. Yuferev, I.A. Tolkachev, V.S. Kalinovsky. Pisma v ZhTF, **50** (1), 39–42 (2024). DOI: 10.61011/PJTF.2024.01.56925.19674
[19] K.J. Williams, R.D. Esman, M. Dagenais. IEEE Photonics technology letters, **6** (5), 639–641 (1994).

Translated by J.Savelyeva